Morphological and effective transport properties of fixed beds of wood chips: Toward realistic modeling of low-temperature pyrolysis

Clarisse Lorreyte, Pierre Lea, Jean-François Henry, Jérôme Adrien, Éric Maire, Hervé Pron, Jaona Randrianalisoa

Morphological and effective transport properties of fixed beds of wood chips: Toward realistic modeling of low-temperature pyrolysis

Cite as: J. Renewable Sustainable Energy **12**, 013101 (2020); doi: 10.1063/1.5123381
Submitted: 6 August 2019 · Accepted: 13 January 2020 ·
Published Online: 18 February 2020

View Online Export Citation CrossMark

Clarisse Lorreyte,[1] Pierre Lea,[1] Jean-François Henry,[1] Jérôme Adrien,[2] Eric Maire,[2] Hervé Pron,[1] and Jaona Randrianalisoa[1,a)]

AFFILIATIONS

[1]Institut de Thermique, Mécanique, Matériaux (ITheMM, EA 7548), Université de Reims Champagne-Ardenne, Campus du Moulin de la Housse, F-51687 Reims, France
[2]Materiaux Ingénierie et Science (MATEIS, UMR 5510), INSA-Lyon, CNRS, Université de Lyon, F-69621 Villeurbanne, France

[a)]jaona.randrianalisoa@univ-reims.fr

ABSTRACT

A detailed understanding of heat transfer and flow is critically important for the pyrolysis of carbonaceous feedstock in fixed bed reactors. In this paper, multimode transport phenomena are simulated by direct pore level simulation on representative digitized samples to retrieve the heat-transfer and pressure-drop properties of highly porous fixed beds of oak-wood chips, which exhibit anisotropic solid-phase tortuosity. A comparison of the direct pore level simulation and simple models of porous media with simple morphologies shows that simple models cannot be used to determine the transport properties of a material with a complex morphology, such as fixed beds of wood chips. Because of drying and devolatilization, the effective thermal conductivity of wood chips decreases with increasing temperature. Heat conduction passes preferentially through the fluid because wood chips have very low thermal conductivity. This study also shows that the shrinking and cracking phenomena resulting from pyrolysis lead to a decrease in the porosity and solid-phase tortuosity and an increase in the specific area. At a high Reynolds number, the pyrolysis also diminishes the permeability but increases the inertial resistance to flow and the interfacial heat transfer.

NOMENCLATURE

A	area, m^2
$A_{f\text{-}s}$	specific area, m^{-1}
c_p	specific heat capacity, $J\,K^{-1}\,kg^{-1}$
D_h	hydraulic diameter, m
d	diameter, m
F	Forchheimer coefficient, m^{-1}
g	gravity constant, m/s^2
K	permeability, m^2
k	thermal conductivity $W\,m^{-1}\,K^{-1}$
L	mean free path, m
Nu	Nusselt number
$\vec{n}$	normal vector
Pr	Prandtl number
p	pressure, Pa
$\vec{q}$	heat flux density, W/m^2
Re	Reynolds number
T	temperature, K
$\vec{u}$	velocity vector, m/s
v#1	volume of 200 × 200 × 200 voxels
v#2	volume of 350 × 350 × 350 voxels
v#3	volume of 400 × 400 × 400 voxels
v#4	volume of 450 × 450 × 450 voxels
v#5	volume of 500 × 500 × 500 voxels
v#6	volume of 600 × 600 × 600 voxels
v#7	volume of 700 × 700 × 700 voxels
wc_s1	wood chips at the initial state
wc_s2	wood chips after a pyrolysis at 573 K

Greek symbols

ε	porosity
μ	dynamic viscosity, Pa s

Π dimensionless pressure gradient
ρ density, kg/m^3
τ tortuosity

Subscripts

a absorbed
D refers to Darcy's law
eff effective
f fluid
in inlet
o outlet
s solid
w wall

Abbreviations

CT Computed tomography
DPLS Direct pore level simulation
RVE Representative volume element

I. INTRODUCTION

Recycling of carbonaceous waste materials and production of syngas via pyrolysis (i.e., thermal decomposition) of biomass are viable routes to increase carbon efficiency and reduce reliance on fossil fuels in the energy and fuel sectors.[1] Pyrolysis is an endothermic process to convert feedstock into volatile matters, tars, and char. Moreover, pyrolysis can be followed by gasification of char through an oxidizing agent.[2,3] Wood chips constitute an abundant waste material in agricultural or in forest regions, and their valorization (e.g., through a thermochemical process) is of vital importance.[4,5]

The modeling of pyrolysis at the reactor scale has attracted attention for many years (see, e.g., Refs. 6 and 7). Such modeling provides a detailed understanding of the contributions of heat and mass transport to kinetics. Moreover, it constitutes a tool for designing efficient reactors. For modeling, heat transfer and flow through the biomass region are characterized for convenience by the "*effective transport properties*," which reflect the multiscale nature of the reactor. Therefore, a better understanding of the effective transport properties (i.e., heat transfer and flow) of biomass such as wood chips is critically important.

Experimentation is undoubtedly the best way to determine such transport properties. Porosity can be determined by weight measurements,[8] the buoyancy method,[9] or mercury intrusion porosimetry.[10] However, because of the pronounced hysteresis between mercury intrusion and extrusion curves, mercury intrusion porosimetry does not provide the total porosity,[11] especially for packed bed materials. Detectable quantities of mercury remain in the samples even after complete pressure release.[10] Collins[12] and Scheidegger[13] overviewed the methods available for determining the specific area of porous media. One such optical-based method determines the ratio of the circumference of the pores to that of the total sectional area, and an adsorption method is based on the assumption that the adsorption of a vapor on a solid surface is related to the exposed surface area. Permeability and the inertial resistance parameter (also called the Forchheimer coefficient[14]) can be estimated by measuring the pressure gradient across the porous medium at various flow velocities.[15]

The thermal conductivity of porous media may be determined by using various methods. A common technique involves two linear probes that are inserted into two parallel holes drilled in the sample.[16] The first probe acts as a heat source and the second as a temperature sensor. Another well-known method is the hot plane (or disk) method,[17] whereby two disks, positioned one on the top and the other on the bottom of the sample, are used to impose a temperature gradient, while flux meters measure the heat flow traversing the sample. However, the hot disk method is less suitable for fixed and packed bed materials because a small contact area leads to significant thermal resistance between the sample and disk surfaces. In this case, the thermal contact resistance dominates the sample thermal resistance, making the latter difficult to estimate with accuracy. The determination of each transport property thus clearly requires a specific experimental device. In addition, biomass samples may undergo morphological changes and devolatilization during the real process. For all of these reasons, the experimental approach is expensive and remains a challenging task.

Alternatively, phenomenological models (see, e.g., Ref. 18) or empirical relations (see, e.g., Refs. 19 and 20) have been proposed. Phenomenological models involve many simplifying physical assumptions and target specific materials that often have simple morphologies, and empirical relations are strongly linked to experimental conditions. These approaches are useful to obtain a first approximation of properties but become clearly inappropriate when (i) the ultimate goal is to obtain quantitative results and (ii) the sample microstructure strongly affects the transport properties.

Numerical modeling combined with a realistic representation of the material is a good alternative approach. Initially, porous media were approximated as a network of spherical pore-bodies connected by cylindrical tubes.[21,22] In porous media with a complex and irregular morphology, the accurate modeling of heat transfer and multi-phase flow has been limited by the lack of information about the microscopic features of these materials. Thanks to the development of the imaging technique of x-ray computed tomography (CT), three-dimensional (3D) representations of porous media are now available and can be used as a direct geometrical input for modeling transport properties. Additionally, the image analysis of digitized samples provides morphological properties such as porosity, specific area, and tortuosity.[23,24]

This study aims to better understand the transport properties of wood chips for use in low-temperature pyrolysis. Toward this end, we used direct pore level simulation (DPLS) of flow and heat transfer through 3D wood-chip samples digitized by x-ray CT imaging. Specifically, DPLS aims to describe the microscopic flow (i.e., solve the Navier–Stokes equations) and solve the energy equations at the pore scale over a representative sample volume, as discussed later in Secs. III to V. Note that the DPLS approach has already been used with success to study the transport properties of various porous media such as tire-waste packed beds,[15] ceramic foams,[14] snow,[25] solar-receiver–based foams,[26] and sandstone rock.[27] Some studies used other numerical methods such as finite-volume–based simulations[28] or pore network modeling.[29,30] Unfortunately, these results are not directly applicable to porous media with different morphologies, such as fixed beds of wood chips. More importantly, the solid material constituting the porous medium in these previous studies was considered a homogeneous medium and characterized by the "bulk-material"

properties. Wood materials consist of vegetal fibers and cylindrical vessels,[31,32] which makes wood a porous medium. We thus report herein the effective thermal conductivity of fixed beds of wood chips, which we obtain by combining DPLS and CT and by using the known properties of the wood from which the chips were made.

The thermal decomposition of feedstock may modify the morphological properties and effective transport properties. Studies on the pyrolysis of waste tires show that it leads to a higher porosity of the packed bed, a higher permeability, but a lower Forchheimer coefficient and Nusselt number.[15] In addition to the determination of structural and effective transport properties, the present study investigates how pyrolysis affects these properties for temperature applications below 573 K.

II. MATERIALS AND CHARACTERIZATION

The selected feedstock is a fixed bed of wood chips (Fig. 1) made from oak hardwood to promote forest-waste reclamation, which is very important for the *Grand–Est* region of France. To estimate how pyrolysis affects the microstructural properties of the packed bed, samples are studied under two conditions: wood chips in their initial state [wc_{s1}, Fig. 1(a)] and wood chips after pyrolysis at 573 K [wc_{s2}, Fig. 1(b)]. Because pyrolysis involves thermal decomposition and devolatilization of the biomass, microstructure modification is expected. The pyrolysis consists of placing the samples in a heating chamber at 573 K for 1 h with a heating rate of approximately 50 K/min (the details of the pyrolysis apparatus are reported elsewhere[33]). At this temperature, the char yield from pyrolysis is about 45%.

A. X-ray computed tomography

Starting in 1990, more realistic representations of pore space became available by the advent of sectioning, confocal laser scanning microscopy, stochastic reconstruction by statistical methods, and, more recently, by x-ray microtomography.[27] The latter was first developed in medicine for imaging soft tissue and bones and was subsequently extended and adapted to a wide variety of industrial tasks. CT is nondestructive and provides images based on the variation of x-ray attenuation within objects.[34] Compared with conventional two-dimensional shadow radiographs where depth information is lost, x-ray tomography provides a complete 3D image because it is constructed from a multitude of radiographic images scanned at different angles.[35]

(a) (b)

FIG. 1. Photographs of samples: (a) in the initial state, wc_{s1}, and (b) after pyrolysis at 573 K, wc_{s2}.

X-ray tomographic imaging was conducted on samples wc_{s1} and wc_{s2}. The scanned samples were placed vertically in cylindrical containers in the same way as in the heating furnace during pyrolysis. X-ray tomography was done by using a v|tome|x, GE Sensing & Inspection Technologies Phoenix X|ray, 160 kV, with a resolution of 15.6 μm.[36] The accuracy of the imaging depends on various factors, such as the resolution and the post-treatment of the scans. Wildenschild *et al.*[35] described the limitations of the CT technique. Some of the most important factors are the artifacts, spatial resolution, and contrast sensitivity. To limit the loss of information from bad contrast and sensitivity, several image-processing steps (e.g., thresholding and binarization obtained by using ImageJ software[37]) were applied to the reconstructed volumes. For these experiments, the threshold level was determined by aligning the numerical porosity with that obtained by the weight measurement method (about 79% for the initial bed of wood chips). The images consist of 1200 × 1200 × 1200 voxels, which correspond to a scanned volume of approximately 1.9 × 1.9 × 1.9 cm^3. As discussed below, such a volume is too big to realize image analysis and DPLS. Thus, an important preliminary step is to determine a smaller numerical volume with properties representative of the entire sample (referred to as a representative volume element, or RVE).

B. Study of a representative volume element

A fundamental approach for determining the effective (morphological and transport) properties is the notion of a RVE. A RVE is defined for each property of interest and corresponds to a volume sufficiently large to capture a representative average value of the given property.[38] To determine the RVE for the morphological properties, seven numerical cubic volumes were studied as reported in Table I.

At the same time, the numerical study of transport properties at the pore scale is computationally expensive (both in terms of time and memory resources). Therefore, DPLS was used for only a limited number and size of sample volumes. Specifically, we studied the permeability and the Forchheimer coefficient of initial wood chips with volumes v#1, v#2, and v#5. Sample v#1 is a very small numerical volume and induces a relatively insignificant computational cost [tens of minutes with an intel (R) Xeon (R) biprocessor computer running at 2.5 GHz and with 64 GB RAM]; v#2 is a moderate numerical volume and induces a reasonable computational cost (about an hour); v#5 is quite a

TABLE I. Seven numerical volumes used to study the RVE for morphological properties.

No.	Volume (voxel unit)
v#1	200 × 200 × 200
v#2	350 × 350 × 350
v#3	400 × 400 × 400
v#4	450 × 450 × 450
v#5	500 × 500 × 500
v#6	600 × 600 × 600
v#7	700 × 700 × 700

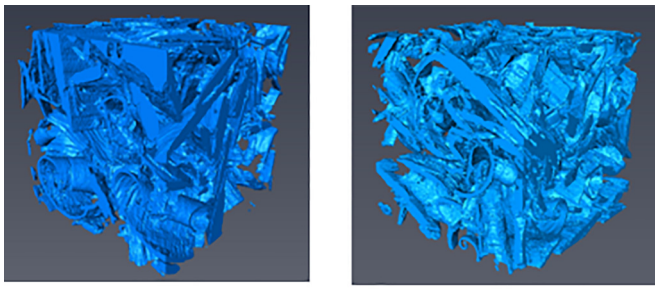

FIG. 2. Three-dimensional rendering of fixed beds of wood chips of v#5: (a) initial state and (b) after pyrolysis at 573 K.

large numerical volume and induces an excessive computational cost (more than a few hours).

Note that pyrolysis reduces the volume of the wood chips, so the RVE size of the sample at the initial stage should be sufficiently large to provide an adequate RVE after pyrolysis. Subsequently, the RVE for initial wood chips (in terms of voxels) was used to investigate the effective properties of samples after pyrolysis (wc_{s2}).

Figure 2 shows a 3D rendering of the wood chip RVE v#5 at the initial state and after pyrolysis. The sample morphology is not qualitatively altered by the low-temperature pyrolysis.

C. Porosity, specific area, and tortuosity

The morphological properties were determined by using image analysis implemented in the software *Imorph*, a cross-platform 3D image analysis software dedicated specifically to porous media.[39] The first step is a macroscopic characterization of the fluid space and the solid phase and directly determines the porosity, tortuosity, and specific area. Figure 3 shows the porosities of different volumes for the initial and pyrolyzed wood chips. Recall that the porosity is the ratio of the volume of air in the packed bed to the total sample volume including solid and gas phases. Porosity is thus dimensionless and ranges from zero to unity for a porous medium. In Figs. 3–5, the side length refers to the length of an edge of the cubic volume. Note from volume v#2 ($350 \times 350 \times 350$ voxels) that the porosity tends to be size-independent, which means that even a quite small volume size provides a good estimate of porosity. Pyrolysis at 573 K does not significantly alter the porosity of the bed, as shown in Fig. 3. The slight decrease in porosity for large volumes can be explained by the shrinkage of wood chips during pyrolysis.[40] In fact, comparing Figs. 1(a) and 1(b) shows that the wood chips contract during drying and devolatilization, so the bed becomes more compact. This reduced porosity can also be due to the modification of the size of meso- and macropores during pyrolysis.[41] As a result, the final sample, consisting mainly of char, has lower porosity.

The specific area of a porous material is defined as the interstitial surface area of the pore either per unit mass or per unit bulk volume of the porous material.[18] Three-dimensional image analysis enables us to estimate this specific area. The Imorph tool uses the marching cube algorithm to determine the total surface area of the solid phase per unit volume (m^{-1}).[39,42] Figure 4 shows the results from the seven volumes studied and an additional volume of size $300 \times 300 \times 300$ voxels. The specific area decreases with increasing volume and converges to a constant value of about 3100 m^{-1} in the limit of large volume. In principle, a larger sample volume corresponds to a more robust result. As a result of the pyrolysis, the specific area increases significantly, as shown in Fig. 4, and reaches a value of about 3800 m^{-1} in the limit of large sample volume. This increase in the specific area is directly linked to the shrinkage effect and to the cracking of the wood chips. The pyrolysis causes some char chips to break into small pieces [see Fig. 1(b)], so the fixed bed becomes more compact, which increases the ratio of the solid surface to the bed volume.

The tortuosity of a fluid space is defined as the ratio of the length along the connected pore channels to the thickness of the porous sample in the main flow direction.[15] Tortuosity is a measure of the deviation of the actual pore structure from an ideal cylinder geometry.[43] The solid-phase tortuosity is defined in a manner analogous to the

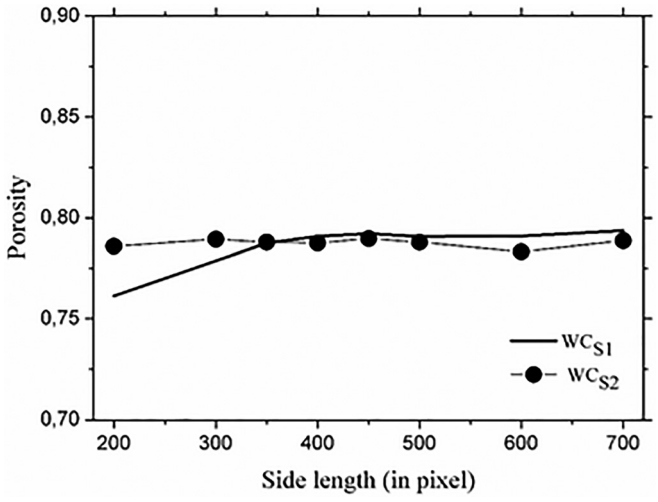

FIG. 3. Porosity of initial and pyrolyzed wood chips in a fixed bed as a function of the side length of cubic volume.

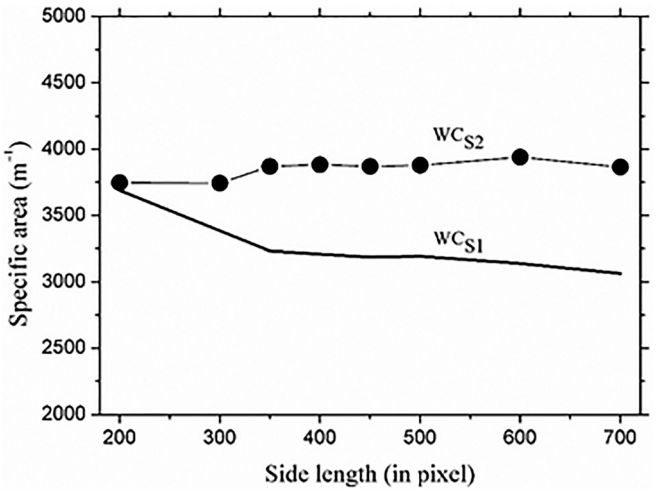

FIG. 4. Specific area of wood chips in initial (thick solid curve) and pyrolyzed (curve plus symbols) states vs the side length of the cubic volume.

fluid-phase tortuosity. The computed tortuosity of the fluid phase is close to unity for different sample volumes, which means that the fluid substance flows easily through the bed of wood chips. This insignificant fluid-phase tortuosity of the current wood chips is not surprising given the high porosity of the bed and the large radius of curvature of wood chips (about 1 cm; see Fig. 1).

Figure 5 shows the tortuosities of the solid phase along the three Cartesian axes. For the initial wood chips, the tortuosity oscillates around 1.25 ± 0.5 in the limit of large volume. Therefore, we chose v#5 as the RVE for the tortuosity analysis. The tortuosity of the solid network is explained by the curved shape of the chips and their weak interconnection (i.e., low number of contact points). The shrinkage effect is relatively weak for low-temperature pyrolysis, and its effect on the tortuosity of a sufficiently large volume (i.e., side length greater than 500 pixels) remains moderate. Specifically, the pyrolysis (or shrinkage) more strongly affects tortuosity in the y direction (the tortuosity decreases from 1.21 to 1.14 when considering only RVE, i.e., a side length from 500 to 700 pixels) than in the x or z direction. The decrease in tortuosity in the y direction could be explained by the shrinkage of the chips in a preferential direction. In other words, during pyrolysis, the chips may be flattened in the y direction and curved in the x and z directions. The solid-phase tortuosity for both initial and pyrolyzed samples is clearly anisotropic, as shown by the fact that the results differ from one direction to another.

The results show that, after the pyrolysis, the porosity and tortuosity slightly decrease, whereas the specific area increases. In other studies, pyrolysis led to an increase in porosity and specific area.[15,44] During the fast pyrolysis of a fixed bed of safflower seeds,[44] the char became more porous, especially at higher temperature (973 K), and the specific area increased between 673 and 873 K. In another example, the pyrolysis of a packed bed of waste tires[15] caused the release of volatile matters, which led to an increase in porosity. At the same time, packed beds of waste tire exhibit a lower tortuosity after the pyrolysis. By studying coal char pyrolysis, Johnsson *et al.*[43] showed that the tortuosity increases with porosity. Guidicianni *et al.*[45] studied the pyrolysis of cellulose, hemicellulose, and lignin and reported a decrease in porosity during pyrolysis, which they attributed to the deposition of carbonaceous species inside the char pores and to a higher yield of the solid residue after the pyrolysis.

This discussion shows that no unique tendency dominates the morphological features of fixed and packed bed materials during thermal decomposition, which highlights the importance of systematically determining the morphological properties for non-regular packed bed samples such as wood chips.

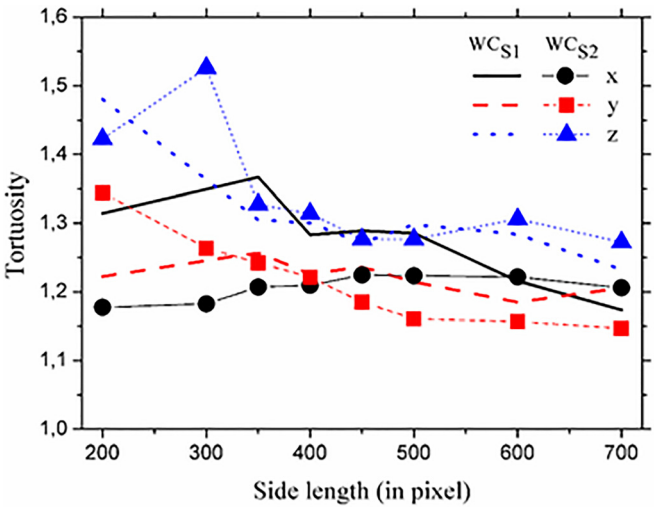

FIG. 5. Solid-phase tortuosity of the initial (curves) and pyrolyzed samples (curves plus symbols) along the three Cartesian axes vs the side length of the cubic volume.

III. DETERMINATION OF PRESSURE DROP: PERMEABILITY AND THE FORCHHEIMER COEFFICIENT

A. Method

Permeability can be used to estimate the ability of fluids to flow through a porous medium. In the present case, it provides a measure of resistance to gas flow through a packed bed under conditions below minimum fluidization.[46] As discussed in the Introduction, we use pore-level simulations of fluid flow through a representative volume of wood-chip samples to determine the effective transport properties, such as permeability and the Forchheimer coefficient.

For a DPLS of fluid flow through a fixed bed, the computational domain consists of an inlet channel, the porous volume, and an outlet channel (see Fig. 6). The inlet and outlet channels ensure homogeneous and undisturbed flows upstream and downstream of the porous medium. In a preliminary study, the lengths of the inlet and outlet channels were determined to be about $0.8L_{RVE}$ and L_{RVE}, respectively, where L_{RVE} is the side length of the RVE along the flow direction (details can be found in Ref. 47). Note that previous studies have also reported that inlet and outlet domains about the size of the sample suffice to ensure homogeneous temperature and flows upstream and downstream of a porous sample.[14,25,48,49] The entire computational domain is discretized into tetrahedral elements by using a mesh generator (Avizo FEI[50]). To define the best compromise between the size of the mesh and the computational cost, a parametric study was done on three different meshes (element edges of 4.60, 4.78, and 5.56 pixels). For two typical Darcy Reynolds numbers (1 and 100), we studied how the mesh size affects pressure, temperature, and heat flux. The main difference between the three meshes appears in the pressure.

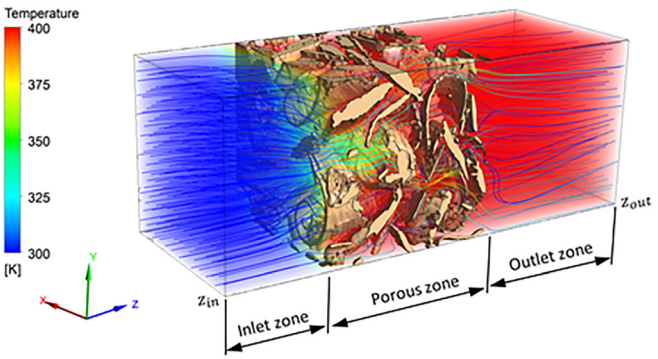

FIG. 6. Schematization of the computational domain comprising inlet, porous, and outlet zones. Typical DPLS of temperature map and velocity streamlines resulting from the flow of a cold fluid (at 300 K and 0.1 m/s^{-1}, i.e., $Re_D = 10$) through a fixed bed of wood chips at 400 K.

An intermediate mesh was chosen for the present study because the results differ from those obtained with the finest mesh by less than 5%, and the computation time is reduced by a factor of two.

ANSYS-Fluent is a CFD software that uses the finite-volume method[51] and is used herein to solve coupled Navier–Stokes and energy equations over the fluid space. Under the *laminar flow regime* hypothesis and in the absence of thermal radiation and other volumetric heat sources, these transport equations are[14,49]

$$\frac{\partial \rho}{\partial t} + \nabla(\rho \vec{u}) = 0, \tag{1}$$

$$\rho\left[\frac{\partial \vec{u}}{\partial t} + (\vec{u}\cdot\nabla)\vec{u}\right] = -\nabla p + \mu(\Delta\vec{u}) + \rho\vec{g}, \tag{2}$$

$$\rho C_p\left[\frac{\partial T}{\partial t} + (\vec{u}\cdot\nabla)T\right] = -\nabla(-k_f \nabla T). \tag{3}$$

Uniform velocity $\vec{u} = u_{in}\vec{z}$ and temperature $T = T_{in}$ are prescribed at the boundary normal to the flow direction ($z = z_{in}$ in Fig. 6). At the outlet ($z = z_{out}$ in Fig. 6), the flow is exposed to the atmospheric pressure ($p = p_{atm}$) and the axial temperature is assumed to be uniform so that the heat flux normal to the outlet boundary is zero ($\vec{q}\cdot\vec{z} = 0$). Symmetry conditions ($\vec{\tau}\cdot\vec{z} = 0$ and $\vec{q}\cdot\vec{n} = 0$ with $\vec{n} = \vec{x}$ or $\vec{y}$ being the unit vector normal to the boundary) are applied at the four lateral boundaries. Finally, the temperature of the solid wet wall is set at $T = T_w$, and no-slip conditions are applied for the velocity field ($\vec{u}\cdot\vec{n} = 0$).

Figure 7 shows typical (relative) pressure profiles along the flow direction (i.e., along the $\vec{z}$ axis in Fig. 6) for different inlet velocities corresponding to different Darcy Reynolds numbers, Re_D, which is defined by

$$Re_D \equiv \frac{u_D D_h}{\nu}, \tag{4}$$

with $u_D = \varepsilon|\vec{u}|$ being the Darcy velocity, which is related to the mean velocity $|\vec{u}|$ within the pores, and D_h being the hydraulic diameter of the pore space. D_h is defined as[18]

$$D_h \equiv 4\frac{V}{S}, \tag{5}$$

where V is the volume of fluid inside the porous volume and S is the wet area of the wood chips. Actually, the pressure values in Fig. 7 represent the pressure averaged over the cross-sectional area of the fixed bed normal to the flow direction. In our calculations, the fluid is air with inlet temperature $T_{in} = 300$ K. The wood chips are hot with a uniform wall temperature $T_w = 400$ K. Note that the pressure drop increases with flow velocity. The pressure decreases very slowly along the inlet zone, then varies abruptly inside the porous zone, and finally approaches atmospheric (relative) pressure in the outlet zone away from the porous boundary.

Figure 8 shows the pressure gradient across the fixed bed samples before (wc_{s1}) and after (wc_{s2}) pyrolysis obtained from the DPLS as a function of the flow velocity (or the Darcy Reynolds number). Note that this figure uses a dimensionless form of the pressure gradient, defined as $\Pi = (-\nabla p \rho D_h^3)/\mu^2$. The results lead to the following observations:

- For low velocity ($Re_D < 1$), the dimensionless pressure gradient varies linearly with Re_D, which is known as the Darcy regime. This means that kinetic energy is not meaningful, and consequently, inertial effects are negligible compared with viscous effects.
- When the flow velocity increases ($Re_D > 10$), the pressure gradient increases proportionally to Re_D^2. In this case, inertial effects become important and overtake viscous effects. Inertial effects are more effective for wood chips after pyrolysis [i.e., wc_{s2} in Fig. 8(b)].
- Comparing the pressure gradients for volumes v#1, v#2, and v#5 [Fig. 8(a)] shows qualitatively that a volume of 350 × 350 × 350 voxels (i.e., sample v#2) could constitute a representative volume for the analysis of flow through the fixed bed of wood chips.

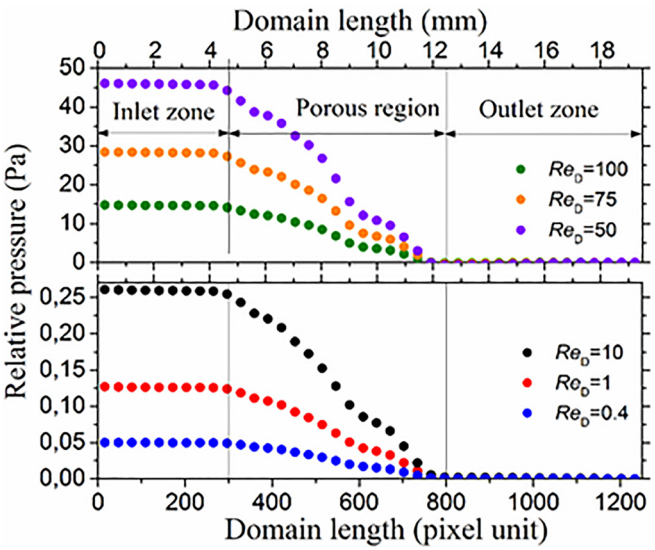

FIG. 7. Pressure gradient through the bed of wood chips for volume v#5 and for six different Darcy Reynolds numbers.

Instead of solving the transport equations (1) and (2) at the pore scale, the flow in the porous medium is frequently modeled by the Darcy–Brinkman–Forchheimer[52] equation or the Darcy–Forchheimer equation.[53] In these models, the porous medium is treated as an isotropic and macroscopically homogeneous system and is characterized by its effective transport properties. The simplest and most frequently adopted model is the well-known Darcy law,[54] which linearly links the pressure drop to the flow velocity weighted by the inverse of the permeability, $1/K$. Darcy's approximation is only valid for low flow velocity (typically for $Re_D < 1$[55]). When the velocity increases ($Re_D > 1$), the inertial resistance becomes comparable to the surface drag because of friction, in accordance with the DPLS results in Fig. 8. An additional term taking into account the inertial resistance through the Forchheimer coefficient F[56] is then added to Darcy's law. This modified Darcy law was initially proposed by Forchheimer[56] and Dupuit[57] and can be expressed as[58]

$$\nabla p = \frac{-\mu}{K} u_D - F\rho u_D^2. \tag{6}$$

The suitability of the Darcy–Forchheimer model (6) has been the subject of intense investigations, as mentioned in Ref. 59. The

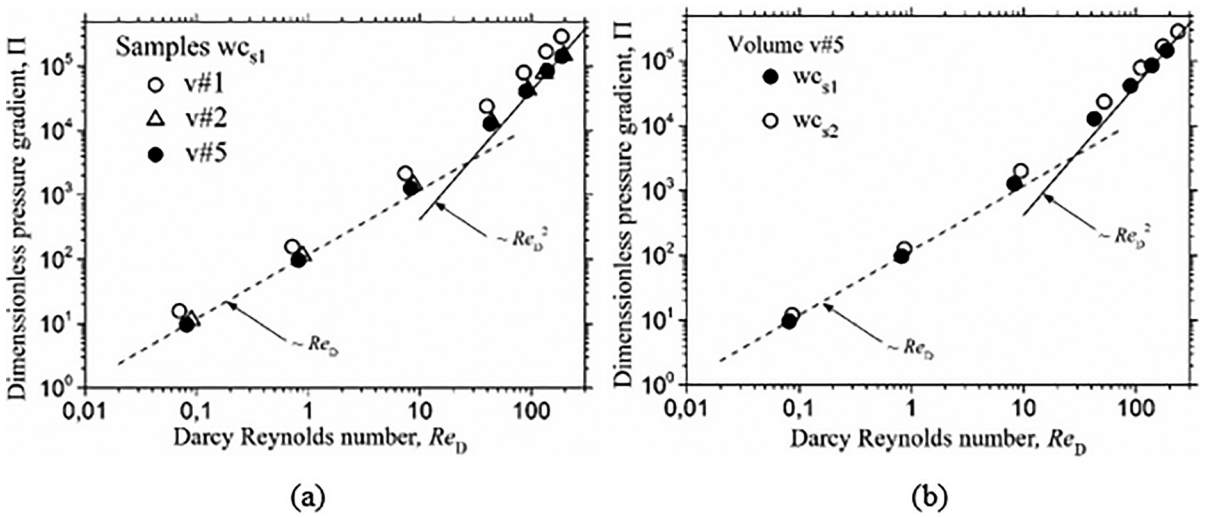

FIG. 8. Dimensionless pressure gradient vs Darcy Reynolds number. (a) Effect of volume of the fixed bed of wood chips in initial state wc_{s1} and (b) effect of thermal treatment for an identical volume v#5.

Darcy–Brinkman–Forchheimer model is reported to be superior in general to the Darcy–Forchheimer model because the latter fails to ensure velocity continuity at the boundaries of the porous medium.[52,60] However, the simplicity of the Darcy–Forchheimer model makes it the most popular model for moderate flow regimes ($Re_D < 300$), as noted in Ref. 61. Using the definition of the dimensionless pressure gradient, Eq. (6) can be rewritten as

$$\Pi = c_0 Re_D + c_1 Re_D{}^2, \tag{7}$$

with $c_0 = D_h^2/K$ and $c_1 = FD_h$.

In this study, we determined the permeability K and the Forchheimer coefficient F (i.e., inertial resistance parameter) by adjusting Eq. (7) to the DPLS data shown in Fig. 8. The corresponding results for K and F are reported in Tables II and III. We now discuss how the sample volume affects the permeability and Forchheimer coefficient (Table II: The values calculated for a volume of $350 \times 350 \times 350$ voxels and a volume of $500 \times 500 \times 500$ differ by 22%). When the sample volume analyzed is too small (e.g., about 200 pixels in our case), its morphological features (porosity, tortuosity, …) and consequently the flow properties may differ from those calculated for larger volumes, as shown in Figs. 3–5. Given that the permeability and Forchheimer coefficient can be approximately expressed as functions of the morphological parameters [see, e.g., Eqs. (8)–(11) below], the permeability and Forchheimer coefficient are clearly affected by the sample volume when the volume is small. In principle, above a certain threshold volume, the so-called RVE, the flow becomes statistically homogeneous, and consequently, the bed volume no longer affects the flow parameters. The volume providing the best compromise between accuracy and computation cost for the pressure-drop properties, which we consider here as the RVE for transport properties, is then clearly $500 \times 500 \times 500$ voxels (i.e., sample v#5).

Based on the above analysis, the DPLS of wood chips after pyrolysis was done for volume v#5. The results (see Table III) show that pyrolysis decreases the permeability but increases the Forchheimer coefficient, which means that the pyrolysis (i.e., specifically the shrinkage here) tends to increase both viscous and inertial resistance to the flow. This trend is consistent with the significant increase in the specific area, in other words, a pyrolysis-induced reduction of particle (chip pieces) and pore size, as shown in Fig. 3. In fact, the decrease in pore size results in a greater pressure drop and inertial resistance to flow.[15] Note that other studies have also reported that pyrolysis affects transport properties such as permeability.[25]

TABLE II. Permeability and Forchheimer coefficient determined from DPLS data for three different volumes of beds of wood chips in the initial state.

Volume No.	v#1	v#2	v#5
K (m^2) $\times 10^{-9}$	3.03	6.24	10.6
F (m^{-1})	5450	2620	2150

B. Comparison with the literature

We now compare the computed values of the parameters K and F with the results from relevant empirical and phenomenological models. Specifically, we compare the following three models of the permeability corresponding to three different morphologies of packed beds:

TABLE III. Permeability and Forchheimer coefficient determined from DPLS data for the bed of wood chips in the initial state (wc_{s1}) and bed of wood chips after pyrolysis (wc_{s2}), both of volume v#5.

Sample Id.	wc_{s1}	wc_{s2}
K (m^2) $\times 10^{-9}$	10.6	6.62
F (m^{-1})	2150	2780

- The Hagen Poiseuille model for porous media composed of parallel channels (straight tubes)[62]

$$K_{HP} = \frac{\varepsilon d^2}{32}, \tag{8}$$

where d is the mean pore diameter.

- The Carman–Kozeny model, also known as the hydraulic radius model[62]

$$K_{CK} = \frac{\varepsilon D_h^2}{36 k_0 \tau}, \tag{9}$$

where k_0 is the Kozeny constant and τ is the tortuosity. For a packed bed of spheres, the product $k_0\tau \approx 5$.

- The third model is the Rumph–Gupte correlation, which was developed for spherical particles[63]

$$K_{RG} = \frac{\varepsilon^{5.5} d^2}{5.6}. \tag{10}$$

For the comparative study of the inertial resistance parameter, we chose the following two correlations:

- The first correlation is based on Ergun's theory and was adapted for a packed bed of spheres by Macdonald *et al.*[64] Note that this model was developed by considering high Reynolds numbers

$$F_M = 1.8 \frac{1-\varepsilon}{\varepsilon^3} \frac{1}{D_h}. \tag{11}$$

- The second model was proposed by Ward for the samples of spherical and granular porous media

$$F_W = \frac{0.55}{\sqrt{K}}. \tag{12}$$

Note that the inertial resistance parameter is independent of the bed porosity in Ward's model.[65]

Figure 9 compares our DPLS results for permeability and the Forchheimer coefficient for wood chips in the initial state and after pyrolysis at 573 K with values obtained from the simple models listed above [i.e., Eqs. (8)–(12)]. The results obtained from the DPLS are of the same order of magnitude as the results from the analytical models, which show clearly that our DPLS method provides meaningful results. However, discrepancies appear between the present results and those from the simple approaches. The Forchheimer coefficients for wood chips lie between the results of the Macdonald and Ward models, whereas the results for permeability are clearly overestimated by all the simple models listed above. This is not surprising because the microstructure of a porous medium strongly influences its flow characteristics.[66–68] Recall also that wood chips have a particular and complex morphology (see Figs. 1 and 2), whereas models (8)–(12) consider beds of spherical or cylindrical particles. This comparison shows clearly the importance of using an appropriate model to determine the flow characteristics of a porous medium with a complex morphology.

IV. CALCULATION OF THE INTERFACIAL HEAT-TRANSFER COEFFICIENT

A. Method

In this section, we use the DPLS as an alternative to experimentation and (phenomenological and empirical) models to determine the heat-transfer characteristics of fluid flow in fixed beds of wood chips. We compute the heat flux over the wet area of the wood chips and the fluid temperature distribution by solving the microscopic transport equations (1)–(3) for the porous sample. It is then straightforward to estimate the heat-exchange parameter between the flowing fluid and solid wall. Specifically, we analyzed the Darcy Nusselt number ($Nu_D = h_{fs} D_h / k_f$, where h_{fs} is the interfacial heat-transfer coefficient, D_h is the hydraulic diameter, and k_f is the fluid thermal conductivity). The energy balance at the wet pore wall leads to

$$Nu_D = \frac{q_w}{\Delta T_{lm}} \frac{D_h}{k_f}, \tag{13}$$

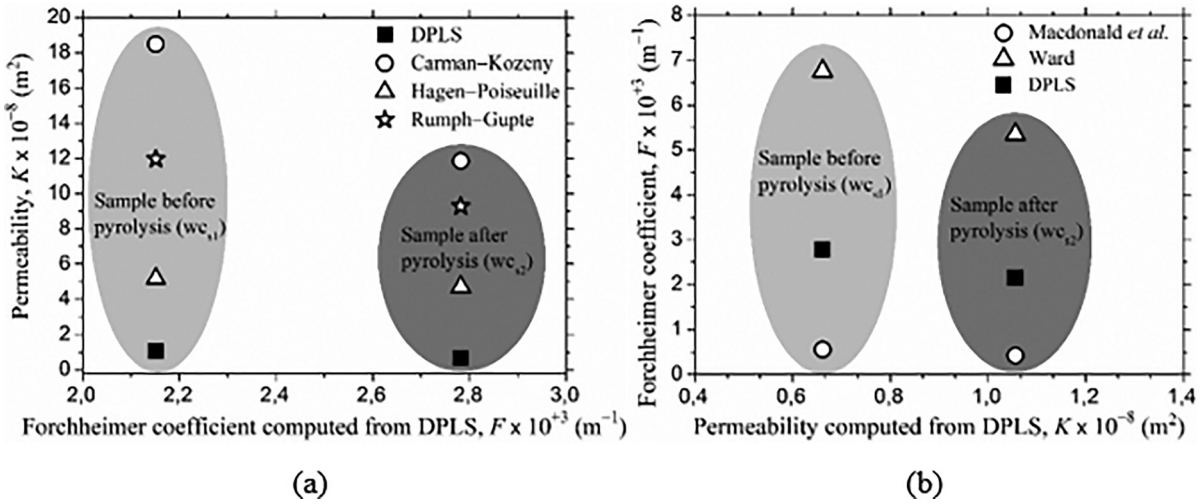

FIG. 9. Comparison of (a) permeability and (b) Forchheimer coefficient obtained from the DPLS and from the simple models (8)–(12).

where q_w is the heat flux over the wet area of the wood chips and ΔT_{lm} is the well-known logarithmic temperature difference, which is commonly used in the field of heat exchangers.[69] When applied to porous media such as foams, ΔT_{lm} takes the form[15]

$$\Delta T_{lm} = \frac{T_w - T_{in}}{ln\left(\frac{T_w - T_{in}}{T_w - T_{out}}\right)}, \tag{14}$$

where T_{in} is the fluid temperature at the bed entrance, T_{out} is the temperature at the exit of the bed, and T_w is the solid wall temperature.

The Nusselt number was calculated only for the volume of $500 \times 500 \times 500$ voxels (i.e., v#5) because the study of the pressure drop shows that this volume constitutes the RVE if the flow characteristics are considered. Figure 10(a) shows the results of the DPLS for wood chips in the initial state and after pyrolysis. The Nusselt number increases with Reynolds number Re_D as $Re_D^{0.62}$ and $Re_D^{0.68}$ for the sample in the initial state and after pyrolysis, respectively. The exponents are consistent with those obtained for foams[14,70] and packed beds of spherical particles.[69,71,72] Note that, for a low Reynolds number (Re_D<100), the Nusselt number (i.e., fluid-solid heat exchange) does not change noticeably upon the pyrolysis of wood chips, probably because morphological modifications are not sufficiently significant to affect the heat exchange between the solid and fluid phases. We notice, however, that, for a high Reynolds number (Re_D >100), the Nusselt number is much greater for the pyrolyzed sample, which is certainly due to the increase in the specific area and the strong inertial effect resulting from pyrolysis. Haussener *et al.*[15] showed that, for the pyrolysis of tire waste at higher temperature, the Nusselt number decreases as a result of morphological changes. In their case, the pyrolysis decreases the specific surface area; in the case of wood chips, the pyrolysis increases the specific surface area. Thus, we expect the interfacial heat transfer to increase at higher temperatures.

B. Comparison with the literature

Considering now the permeability and Forchheimer coefficient, we compare the Nusselt number obtained from the DPLS with well-known correlations. The first is suggested by Wakao *et al.*[71] and was established for cylindrical and spherical particles and for a Darcy Reynolds number ranging from 4 to 1200,

$$Nu_W = 2 + 1.1[6(1-\varepsilon)]^{0.6} Re_D^{0.425} Pr^{1/3}. \tag{15}$$

A second relationship was proposed by Incropera and Dewitt for a packed bed of cylindrical particles and for a Darcy Reynolds number in the range 20 to 1000,[69]

$$Nu_{ID} = \frac{0.79}{\varepsilon}[6(1-\varepsilon)]^{0.425} Re_D^{0.425} Pr^{1/3}. \tag{16}$$

Finally, we consider a third correlation by Bird *et al.*,[72] which was also developed for a packed bed of cylindrical particles but with a differentiation for low (Re_D< 45) and high (Re_D > 45) Reynolds number

For $Re_D < 45$,

$$Nu_3 = 0.789[6(1-\varepsilon)] Re_D^{0.49} Pr^{1/3}. \tag{17}$$

For $Re_D > 45$,

$$Nu_4 = 0.534[6(1-\varepsilon)] Re_D^{0.59} Pr^{1/3}. \tag{18}$$

Figure 10(b) compares the correlations, Eqs. (15)–(18), with the DPLS results. The DPLS results are of the same order of magnitude as those from the correlations. The results of the model by Bird *et al.* coincide the most with the DPLS results.

V. DETERMINATION OF EFFECTIVE THERMAL CONDUCTIVITIES

For fast transient processes and when both the solid and fluid phases generate heat (both cases would occur during pyrolysis), the local-thermal-equilibrium hypothesis may not be satisfied, so heat

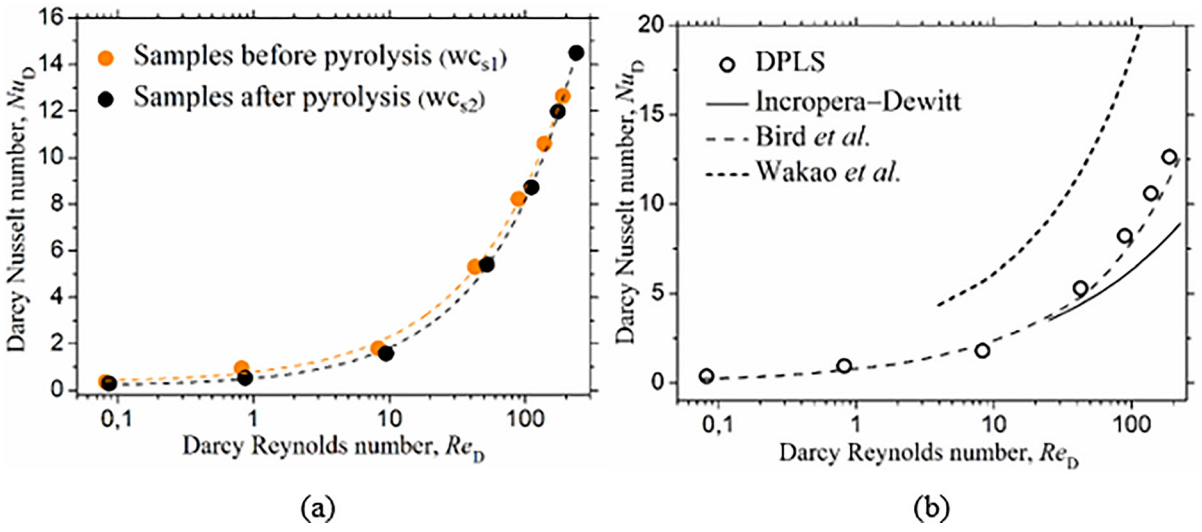

FIG. 10. (a) Darcy Nusselt number from DPLS for wood chips in the initial state compared with that for wood chips after pyrolysis at 573 K and (b) Darcy Nusselt number from DPLS for wood chips in the initial state compared with the Darcy Nusselt number from literature models.

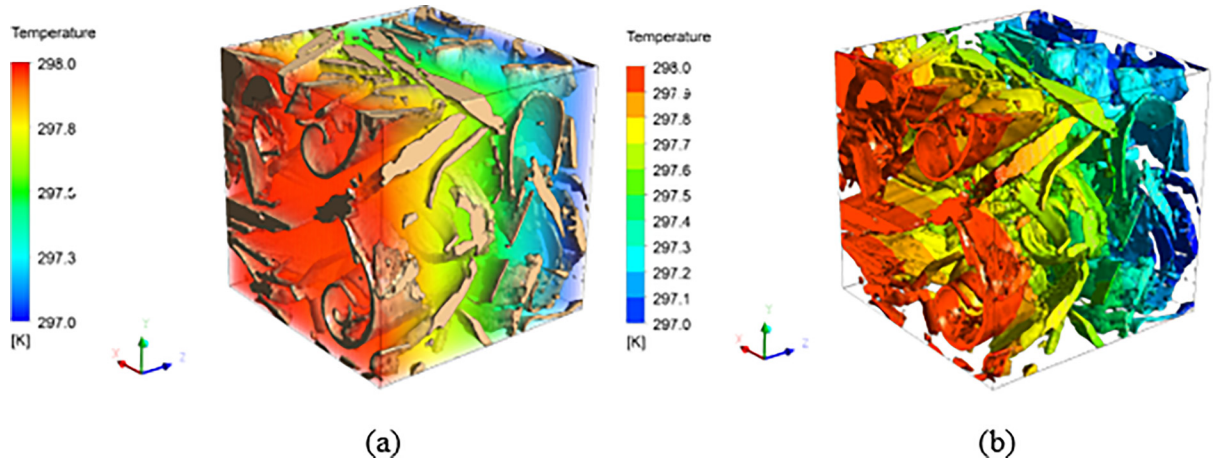

FIG. 11. Schematization of DPLS of heat conduction in (a) tortuous stagnant fluid and (b) fixed bed of wood chips. Based on the previous flow and heat-transfer analysis, the RVE was taken as a sample volume of 500 × 500 × 500 voxels. The color bar indicates the temperature distribution as a result of an applied temperature difference $T_{hot} - T_{cold}$ across the system.

transfer in the porous system should be analyzed by a two-temperature treatment.[62] Such a treatment, also called the non-local-thermal-equilibrium approach, requires the effective thermal conductivity of each phase and the heat-exchange coefficient between the fluid and the solid phases, as discussed in Sec. IV A.

We applied the DPLS method because the experimental determination of the thermal conductivity of fixed and packed beds remains challenging and no suitable model exists for a bed of wood chips. To simplify the situation, we assume that the fluid is stagnant in the bed of wood chips, which implies that thermal dispersion is neglected and that heat transfer in the fluid phase is driven by heat conduction and, thus, is independent of flow velocity. Note that Hsu and Cheng, among others, derived a theoretical approach to model thermal dispersion in a porous medium of simple geometry.[73] Based on the stagnant-fluid assumption, the DPLS solves separately the equation for microscopic energy in the fluid phase [Eq. (19a)] and in the solid phase [Eq. (19b)]. Figure 11 depicts the computational domains associated with the volume of 500 × 500 × 500 voxels. The two opposite boundaries of the fluid [Fig. 11(a)] and solid [Fig. 11(b)] phases along the z axis have a temperature gradient. The remaining boundaries are adiabatic, so no heat is exchanged between the solid and fluid phases

$$\nabla(-k_f \nabla T) = 0 \quad \text{and} \quad \vec{n} \cdot -k_f \nabla T = 0, \tag{19a}$$

$$\nabla(-k_s \nabla T) = 0 \quad \text{and} \quad \vec{n} \cdot -k_s \nabla T = 0, \tag{19b}$$

where $\vec{n}$ is the unit normal for the solid or the fluid phase boundary of the computational volume.

Equations (19a) and (19b) were solved by using ANSYS-Fluent. The difference between T_{hot} and T_{cold} was set to 1 K to obtain the thermal conductivity at the average temperature. The effective thermal conductivities of the tortuous fluid, $k_{eff,f}$, and of the fixed bed, $k_{eff,s}$, are determined by

$$k_{eff,j} = \frac{L_z}{L_x L_y} \frac{\int_{A_j} \vec{q}_j \cdot \vec{z}\, dA}{(T_{hot} - T_{cold})} \quad (j = f,\ s), \tag{20}$$

where L_x, L_y, and L_z are the sample dimensions along the x, y, and z axes of the Cartesian system. The vector $\vec{q}_j$ is the heat flux at the isothermal boundary of substance j, and $\vec{z}$ is the unit normal along the z axis.

Figure 12 shows the thermal conductivity of each phase as a function of temperature.

On the one hand, the effective thermal conductivity of the stagnant fluid increases with temperature, which is consistent with the thermal conductivity of bulk air at atmospheric pressure.[74] On the other hand, the effective thermal conductivity of the fixed bed decreases with increasing temperature and is at least two- to three-fold less than the effective thermal conductivity of the stagnant fluid. This difference comes from two factors: (i) the complex

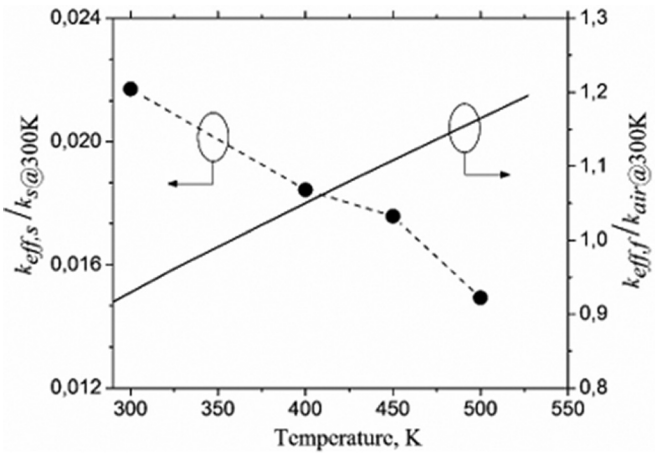

FIG. 12. Dimensionless effective thermal conductivity of a fixed bed of wood chips, $k_{eff,s}$, and of tortuous stagnant fluid, $k_{eff,f}$, vs temperature for sample volume v#5. The notation $k_{eff,s}$@300 K refers to the thermal conductivity of the initial oak wood (equates to 0.19 W m^{-1}K^{-1}), and k_{air}@300 K is the thermal conductivity of air at ambient conditions (about 0.026 W m^{-1}K^{-1}).

morphology of the fixed bed and (ii) intrinsic features of the wood chips. First, the beds of wood chips have very high porosity (about 79%–86% depending on the thermal treatment, see Fig. 3), a tortuous nature, and weak connectivity (featured by a tortuosity of about 1.5 in the z direction for sample v#5, see Fig. 5). In this case, the thermal conductivity of the wood itself involved in Eq. (19b) is extremely low, as discussed below.

To obtain a realistic value of the thermal conductivity k_s of wood chips, we measured the thermal conductivity of the bulk oak wood from which wood chips were made. We studied four disks of oak wood with thicknesses ranging from 2.50 to 10.09 mm. The thermal measurement instrument used the hot plate method and consisted of a heat source and a heat sink placed above and below each wood disk, which maintained a constant temperature difference of about 10 K between the two sides of each disk. A flux meter was inserted between the heat source and the sample and another between the sample and the heat sink. The flux meters measured the heat flow passing through the sample between the heat source and sink. See our previous report for a detailed description of the experimental setup.[75] Measuring the heat flux through varying sample thicknesses gives the curve of overall thermal resistance R_{tot} vs thickness L_z. The thermal conductivity corresponding to the four oak wood samples was obtained by fitting the following equation to the experimental data:

$$R_{tot}(L_z) = \frac{q(L_z)}{T_{hot} - T_{cold}} = \frac{L_z}{k_s} + R_c, \tag{21}$$

where R_c is the thermal contact resistance between the flux meters and the sample and can be obtained from the fit.

Four sets of measurements were done to obtain the thermal conductivity of the oak wood, which underwent different thermal treatments. In the first case, the wood at the initial state was wet (about 10% moisture content). In the other three cases, the four samples of different thicknesses were successively dried in an electric oven for 24 h at 373, 423, and 473 K. Drying was not done above 473 K because it requires drying under a neutral gas to avoid char oxidation, and no such device was available. The thermal conductivity of the oak wood varies from 0.19 down to 0.13 W $m^{-1}K^{-1}$ for wood in the initial state and wood dried at 473 K. The thermal conductivity of dried wood is less than that of the initially wet wood because of the contribution of water molecules. The thermal conductivity of water is about 0.6 W $m^{-1}K^{-1}$.[74] These results for oak wood are consistent with data for various woods. For example, the thermal conductivity of pine, lime tree, elderberry tree, and oak from Mongolia were measured to be about 0.10, 0.12, 0.11, and 0.19 W $m^{-1}K^{-1}$, respectively.[76]

VI. CONCLUSION

We investigate herein the morphological and effective transport properties of fixed beds of wood chips by using a combination of x-ray tomographic imaging and direct pore level simulation (DPLS). The relevant morphological properties, namely, porosity, specific area, and tortuosity, of the fixed beds were determined from the three-dimensional image analysis of the representative volume element (RVE) to obtain results representative of materials used in practice. The experimental results of a low-temperature pyrolysis at about 573 K show a char yield of about 45% and a gas production mainly composed of CO_2. Additionally, three-dimensional rendering of the pyrolyzed sample shows that pyrolysis shrank some wood chips and broke others. The beds of wood chips exhibit anisotropic solid-phase tortuosity, whereas the fluid-phase tortuosity is negligible. Pyrolysis causes a slight decrease in porosity and in the solid-phase tortuosity and a significant increase in the specific area. The permeability and Forchheimer coefficient obtained from the DPLS are qualitatively consistent with the results of several simple phenomenological models. At the same time, these simple models are not appropriate to determine the pressure-drop properties of fixed beds of complex-morphology wood chips. During the pyrolysis of wood chips, the permeability decreases, whereas the inertial resistance increases. The Nusselt number increases with the Reynolds number as $Re_D^{0.62}$ for wood chips in the initial state and as $Re_D^{0.68}$ for wood chips after pyrolysis at 573 K. This result shows the slight effect pyrolysis has on the heat exchange between the air flow and the wood chips. Between 293 and 473 K, the effective thermal conductivity of wood chips decreases with increasing temperature because of drying and devolatilization of chemical species. Comparing the effective thermal conductivities of wood chips and stagnant air allows us to conclude that the heat conduction is done through the air molecules because of very low thermal conductivity of tortuous and weakly connected wood chips.

ACKNOWLEDGMENTS

This study was supported by the Essaimage grant of the Region Champagne-Ardenne and the APR grant of the "Structure Fédérative de Recherche (SFR) Condorcet" to H.P. and J.R. The authors are grateful to Professor Sophia Haussener from the EPFL (Lausanne, Switzerland) for fruitful discussions. The authors gratefully acknowledge the High-performance Computing (HPC) resources that were used for this research and made available through the ROMEO Computing Center hosted by the University of Reims Champagne-Ardenne.

REFERENCES

[1]D. Sutton, B. Kelleher, and J. R. Ross, "Fuel process," Technol. **73**, 155 (2001).
[2]W. Zhu, W. Song, and W. Lin, Fuel process. Technol. **89**, 890 (2008).
[3]E. Cetin, B. Moghtaderi, R. Gupta, and T. F. Wall, Fuel **83**, 2139 (2004).
[4]A. Demirbaş, Energy Convers. Manag. **42**, 1357 (2001).
[5]A. V. Bridgwater and G. D. Evans, "Energy technology support unit (Great Britain), and Great Britain. Department of trade and industry," *An Assessment of Thermochemical Conversion Systems for Processing Biomass and Refuse* (Harwell Laboratory, Energy Technology Support Unit, 1993).
[6]S. S. Alves and J. L. Figueiredo, Chem. Eng. Sci. **44**, 2861 (1989).
[7]B. V. Babu and A. S. Chaurasia, Energy Convers. Manag. **44**, 2251 (2003).
[8]L. Y. Mwaikambo and M. P. Ansell, J. Mater. Sci. Lett. **20**, 2095 (2001).
[9]E. J. W. Visser and G. M. Bögemann, Plant Soil **253**, 81 (2003).
[10]P. Klobes, H. Riesemeier, K. Meyer, J. Goebbels, and K.-H. Hellmuth, Fresenius J. Anal. Chem. **357**, 543 (1997).
[11]C. Galle, Cem. Concr. Res. **31**, 1467–1477 (2001).
[12]R. E. Collins, *Flow of Fluids through Porous Materials* (Van Nostrand Reinhold, New Jersey, 1961).
[13]A. Scheidegger, *The Physics of Flow through Porous Media* (University of Toronto Press, Toronto, 1974).
[14]J. Petrasch, F. Meier, H. Friess, and A. Steinfeld, Int. J. Heat Fluid Flow **29**, 315 (2008).
[15]S. Haussener, I. Jerjen, P. Wyss, and A. Steinfeld, J. Heat Transfer **134**, 012601 (2012).
[16]K.-H. Kim, S.-E. Jeon, J.-K. Kim, and S. Yang, Cem. Concr. Res. **33**, 363 (2003).
[17]M. Khandelwal and M. M. Mench, J. Power Sources **161**, 1106 (2006).
[18]F. A. L. Dullien, *Porous Media: Fluid Transport and Pore Structure*, 2nd ed (Academic Press, San Diego, 1992).

[19]C. Di Blasi, AIChE J. **50**, 2306 (2004).
[20]G. Mavko, T. Mukerji, and J. Dvorkin, *The Rock Physics Handbook: Tools for Seismic Analysis of Porous Media*, 2nd ed. (Cambridge University Press, Cambridge, 2009).
[21]G. R. Jerauld and S. J. Salter, Transp. Porous Media **5**, 103 (1990).
[22]J. Koplik, C. Lin, and M. Vermette, J. Appl. Phys. **56**, 3127 (1984).
[23]D. M. L. Cooper, J. R. Matyas, M. A. Katzenberg, and B. Hallgrimsson, Calcif. Tissue Int. **74**, 437 (2004).
[24]Y. Nakashima and S. Kamiya, J. Nucl. Sci. Technol. **44**, 1233 (2007).
[25]E. Zermatten, M. Schneebeli, H. Arakawa, and A. Steinfeld, Cold Reg. Sci. Technol. **97**, 33 (2014).
[26]S. Du, Z.-X. Tong, H.-H. Zhang, and Y.-L. He, Renewable Energy **135**, 711 (2019).
[27]S. Ovaysi and M. Piri, J. Comput. Phys. **229**, 7456 (2010).
[28]A. Q. Raeini, B. Bijeljic, and M. J. Blunt, Adv. Water Resour. **83**, 102 (2015).
[29]S. M. Shah, F. Gray, J. P. Crawshaw, and E. S. Boek, Adv. Water Resour. **95**, 276 (2016).
[30]R. Song, J. Liu, and M. Cui, Int. J. Heat Mass Transfer **109**, 705 (2017).
[31]R. Patt, O. Kordsachia, and J. Fehr, Wood Sci. Technol. **40**, 39 (2006).
[32]L. Dombrovsky, J. F. Henry, C. Lorreyte, H. Pron, and J. Randrianalisoa, Appl. Opt. **57**, 6657–6663 (2018).
[33]C. Lorreyte, J. Randrianalisoa, C. Gennequin, J.-F. Henry, E. Abi Aad, and H. Pron, "Experiemental study of the pyrolysis of wood chips," Energies (submitted).
[34]R. A. Ketcham and W. D. Carlson, Comput. Geosci. **27**, 381 (2001).
[35]D. Wildenschild, C. M. P. Vaz, M. L. Rivers, D. Rikard, and B. S. B. Christensen, J. Hydrol. **267**, 285 (2002).
[36]J. Kastner, B. Harrer, G. Requena, and O. Brunke, NDT E Int. **43**, 599 (2010).
[37]T. Ferreira and W. Rasband, *ImageJ User Guide* (2012).
[38]J. Bear, *Dynamics of Fluids in Porous Media* (Courier Corporation, 2013).
[39]E. Brun, J. Vicente, F. Topin, and R. Occelli, "Imorph: An open source software for 3D structural and geometrical analysis of porous media," Conference Paper, Metfoam 09, Bethesda, MD (2009).
[40]K. O. Davidsson and J. B. C. Pettersson, Fuel **81**, 263 (2002).
[41]P. Fu, S. Hu, J. Xiang, L. Sun, S. Su, and J. Wang, J. Anal. Appl. Pyrolysis **98**, 177 (2012).
[42]W. Lorensen and H. Cline, Comput. Graph. **21**, 163–169 (1987).
[43]J. E. Johnsson and A. Jensen, Proc. Combust. Inst. **28**, 2353 (2000).
[44]O. Onay, Fuel Process. Technol. **88**, 523 (2007).
[45]P. Giudicianni, G. Cardone, and R. Ragucci, J. Anal. Appl. Pyrolysis **100**, 213 (2013).
[46]*Multiphase Flow Handbook*, 2nd ed., edited by E. E. Michaelides, C. T. Crowe, and J. D. Schwarzkopf (CRC Press/Taylor & Francis Group, Boca Raton/London.New York, 2017).
[47]C. Lorreyte, "Etudes numérique et expérimentale de la synthèse de biogaz: Vers la transformation thermochimique solaire de copeaux de bois," Thèse de doctorat (Université Reims Champagne Ardennes, 2017).
[48]S. M. Moosavi, M. Niffeler, J. Gostick, and S. Haussener, Chem. Eng. Sci. **176**, 503 (2018).
[49]S. Haussener, "Tomography-based determination of effective heat and mass transport properties of complex multi-phase media," PhD dissertation (ETH Zurich, 2010).
[50]C. Lore, *Thermo Scientific Avizo Software 9* (ACM, 2018).
[51]T. A. Stolarski, Y. Nakasone, and, and S. Yoshimoto, *Engineering Analysis with ANSYS Software*, 2nd ed. (Butterworth-Heinemann, Oxford, 2018).
[52]K. Vafai and S. J. Kim, Int. J. Heat Fluid Flow **16**, 11 (1995).
[53]D. A. Nield, Int. J. Heat Fluid Flow **12**, 269 (1991).
[54]H. Darcy, *Les Fontaines Publiques de La Ville de Dijon* (Victor Dalmont, 1856).
[55]A. Dybbs and R. V. Edwards, in *Fundamentals of Transport Phenomena in Porous Media*, edited by J. Bear and M. Y. Corapcioglu (Springer Netherlands, Dordrecht, 1984), pp. 199–256.
[56]P. Forchheimer, in *Water Movement Ground*, Zeitschrift des Vereins Deutscher Ingenieure, Zeitschrift fur Acker und Pflanzenbau (49, 1901), pp. 1736–1749.
[57]J. Dupuit, *Etudes Théoriques et Pratiques Sur Le Mouvement Des Eaux Dan Les Canaux Découverts et à Travers Les Terrains Perméables* (Dunod, Paris, 1863).
[58]E. Zermatten, S. Haussener, M. Schneebeli, and A. Steinfeld, J. Glaciol. **57**, 811 (2011).
[59]D. A. Nield and A. Bejan, *Convection in Porous Media*, 3rd ed. (Springer, New York, 2006).
[60]G. Amhalhel and P. Furmanski, J. Power Technol. **85**, 55 (1997).
[61]P. Kumar and F. Topin, J. Fluids Eng. **139**, 111401 (2017).
[62]M. Kaviany, *Principles of Heat Transfer in Porous Media* (Springer Science & Business Media, 2012).
[63]Rumpf and Gupte, Chem. Eng. Technol. **43**, 367 (1971).
[64]I. F. Macdonald, M. S. El-Sayed, K. Mow, and F. A. L. Dullien, Ind. Eng. Chem. Fundam. **18**, 199 (1979).
[65]J. C. Ward, *Turbulent Flow in Porous Media* (University of Arkansas, Engineering Experiment Station, 1965).
[66]Y. Jobic, P. Kumar, F. Topin, and R. Occelli, Heat Mass Transfer **54**, 2351 (2018).
[67]J. T. Richardson, Y. Peng, and D. Remue, Appl. Catal. Gen. **204**, 19 (2000).
[68]G. Incera Garrido, F. C. Patcas, S. Lang, and B. Kraushaar-Czarnetzki, Chem. Eng. Sci. **63**, 5202 (2008).
[69]F. P. Incropera and D. P. DeWitt, *Introduction to Heat Transfer*, 2nd ed. (Wiley, New York, 1990).
[70]L. B. Younis and R. Viskanta, Int. J. Heat Mass Transfer **36**, 1425 (1993).
[71]N. Wakao and T. Funazkri, Chem. Eng. Sci. **33**, 1375 (1978).
[72]E. C. Nsofor and G. A. Adebiyi, Exp. Therm. Fluid Sci. **24**, 1 (2001).
[73]C. T. Hsu and P. Cheng, Int. J. Heat Mass Transfer **33**, 1587 (1990).
[74]P. Linstrom, "NIST Chemistry WebBook," J. Chem. Eng. Data **46**, 1059–1063 (2001).
[75]J. Randrianalisoa, J.-F. Henry, and D. Caron, "Acte de congrès," *Thermique, Mers et Océans* (Marseille, France, 2017).
[76]Y. Qing-Xian, J. For. Res. **12**, 43 (2001).